Materials and Design 196 (2020) 109124

Contents lists available at ScienceDirect

Materials and Design

journal homepage: www.elsevier.com/locate/matdes

Combined athermal and isothermal martensite to austenite reversion kinetics, experiment and modelling

H. Kooiker [a,b,*], E.S. Perdahcıoğlu [b], A.H. van den Boogaard [b]

[a] Philips HealthTech, Amstelplein 2, 1096 BC Amsterdam, the Netherlands
[b] University of Twente, Department of Nonlinear Solid Mechanics, Drienerlolaan 5, 7522 NB Enschede, the Netherlands

HIGHLIGHTS

- A novel laser heat treatment setup is introduced that can heat with very high heating and cooling rates.
- A kinetic transformation framework is presented that accounts for both athermal and isothermal α' to γ transformation.
- The kinetic model leads to excellent agreement between prediction and experimental result.

GRAPHICAL ABSTRACT

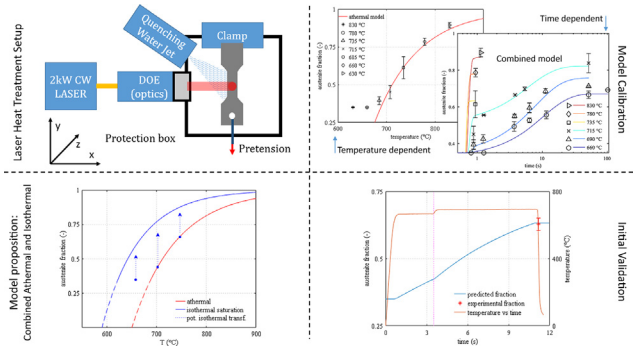

ARTICLE INFO

Article history:
Received 14 July 2020
Received in revised form 29 August 2020
Accepted 3 September 2020
Available online 05 September 2020

Keywords:
Phase reversal
Athermal transformation
Thermally activated transformation
Laser heat treatment
Austenitic stainless steel
Kinetic modelling

ABSTRACT

A novel laser heat treatment setup is presented and used to characterize the reverse transformation of martensite to austenite resulting from highly dynamic laser heat treatments of stainless steel. During laser heat treatments the irradiated spot and its surroundings can experience completely different thermal loads, yet both experience reverse transformation. The experiments are conducted such to reflect these diverse conditions. Next to experiments, a new kinetic model is reported which combines both athermal and isothermal transformation mechanisms to cope with the diversity in conditions in a unified framework. The experimental results show that reverse transformation can proceed extremely fast, yet saturates at intermediate temperatures. Additionally, it is shown that there is good agreement between experiment and model and it is essential to embed both the athermal and isothermal transformation mechanism in the model for achieving this performance. Initial steps towards model validation are performed showing good predictability of a non-isothermal heat treatment with conditions realistic and relevant for industrial laser heat treatments.

1. Introduction

A novel approach to achieve sufficient strength *and* ductility of metastable austenitic stainless steels are local phase reversal (laser-) heat treatments, enabling extreme local tailoring of material properties.

During phase reversal heat treatment the mechanically induced martensite of a cold rolled austenitic stainless steel is reverted back to austenite. Proper execution leads to a fine-grained austenitic structure, with grains in the nano to submicron range imparting excellent room-temperature strength and ductility to the material [1–3]. Cold rolled metastable austenitic stainless steel can experience two types of reverse transformation; an athermal 'shear-type' and an isothermal (thermally activated 'diffusional') reverse transformation [4,5]. Both transformation-types lead to an austenitic lattice, however the resulting microstructures are completely different. Whereas thermally activated

* Corresponding author at: Philips HealthTech, Amstelplein 2, 1096 BC, Amsterdam, the Netherlands.
E-mail address: harm.kooiker@philips.com (H. Kooiker).

https://doi.org/10.1016/j.matdes.2020.109124

isothermal transformation is time dependent and leads to equiaxed finely grained austenite of low dislocation density [5], athermal transformation depends on temperature only and leads to lath-shaped austenite with high dislocation density [6]. The type of reverse transformation that is experienced by an austenitic stainless steel depends on its chemical composition and the heating rate that is applied during the heat treatment [5,7,8]. Higher heating rates and higher temperatures enable athermal transformation, whereas low austenite stability enables isothermal transformation. Dastur et al. [9] and Souza Filho et al. [10] show that diffusional reverse transformation can be governed by the diffusion of Mn. Furthermore, heterogeneity build-up of Ni during the transformation changes local austenite stability and can therefore lead to a two stage transformation process [10]. Because of the differences between isothermal and athermal transformation, both in terms of kinetics and resulting microstructure, it is important to know which type governs the behaviour of a particular transformation.

An important contribution to the understanding of reverse transformation has been provided by Tomimura et al. In 1991 they investigated the reverse transformation mechanisms occurring in a range of austenitic stainless steels of varying chemical composition, including AISI 301 [11]. They presented a criterion to determine if a material *can* experience athermal transformation which is based on the Gibbs free energy difference between ferrite and austenite. Somani et al. refined this criterion by adding the influence of more alloying elements on the free energy difference [12]. This criterion suggests that reverse transformation of AISI 301 is dominated by the athermal mechanism. However, experimental results from others suggest that AISI 301 reversion is in fact dominated by isothermal transformation, e.g. Johanssen et al. subjected AISI 301 to an annealing treatment between 600 °C and 900 °C for 30 min, leading to a temperature dependent transformation type [13]. At temperatures below 800 °C isothermal transformation was found, whereas higher temperatures induced an athermal transformation. Similarly, Di Schino et al. investigated reverse annealing of AISI 301 in the temperature range from 600 °C and 750 °C and found a time-dependent transformation [14]. Importantly, they extended the annealing duration to a maximum of 7 days and thus found evidence of a saturation level, i.e. incomplete transformation.

There is an apparent discrepancy between observed transformation mechanism from one investigation to another. The varying results suggest that both types of transformation are possible and can occur simultaneously. The main difference between the experiments of the cited authors is the equipment with which the heat treatments were executed; resulting in differences in heating rate *and* cooling rate.

To date only a few models have been proposed for the kinetics of reverse transformation. Rajasekhara [15] modelled diffusional transformation of AISI 301LN based on a general kinetics model from Erukhimovitch and Baram [16]. It was specifically developed to investigate the underlying principles of isothermal reverse transformation, particularly the preferential nucleation sites and growth governing diffusion species. Although the model is insightful, it does not show acceptable agreement with the experimental transformation data. Somani et al. also presented a kinetic model capable of modelling isothermal annealing [12], although it is claimed that a good fit is obtained this is not shown in the research itself. Stalder et al. modelled reverse transformation where the transformation was partially athermal and isothermal [17]. Following the Avrami approach, a double Avrami function was fitted, where the characteristic exponent was made dependent on the transformation mechanism.

More recently, other researchers have successfully developed more physically-based models of reverse transformation. Galindo-Nava et al. presented a physics-based modelling framework for the prediction of martensite to austenite reversion kinetics [18]. In their model the kinetics are governed by the diffusivity of the growth governing species Mn and Ni. Importantly, they also consider that diffusional reversion saturates when an equilibrium fraction of austenite is reached. Yeddu et al. developed a 3D physically-based phase-field model for athermal formation of martensite and its reverse transformation into austenite for AISI 301 [19]. Although this model has the potential to provide insight into the kinetics of athermal reverse transformation it is not compared to experimental data. Zhang et al. developed a 2D phase-field model that accounts for both athermal and diffusional reverse transformation [20]. A good asset of this model is the ability to account for ongoing growth of athermally formed austenite. Although the aforementioned phase field models provide a more physically-based view of the reverse transformation process they are not well-suited for the Finite Element based optimization of heat treatment *processes* which requires highly efficient and fast models.

Realistic laser heat treatments include e.g. multiple laser passes by scanning. Optimization of such processes requires models that can predict the transformation for non-monotonic heating that can be of both short-duration high-intensity and long-duration medium-intensity. The models presented in literature thus far fail to meet one or all of the following requirements:

- The model must be designed in rate-form to be able to account for arbitrary non-monotonic thermal load
- The model must be able to account for both athermal and isothermal reverse transformation
- The model must be able to accommodate for the experimentally observed transformation-saturation
- The model must be computationally efficient

In this work a novel experimental setup is employed to conduct high heating-rate laser heat treatment experiments on AISI 301 and thus allows characterization of reverse transformation under conditions that are representative for real industrial laser heat treatments. Next to the experimental characterization a model is presented that combines two existing models and is capable of meeting the aforementioned model-requirements, i.e. predicting the kinetics during arbitrary thermomechanical loading, accounting for both athermal and isothermal transformation and an isothermal transformation saturation. The model is calibrated to the transformation experiments after which an initial robustness check is performed by comparing the model prediction to a non-isothermal temperature 'jump' experiment. Lastly, the added value of the combination of athermal and isothermal kinetics is determined by comparing the model to an approach that accounts for isothermal transformation only.

2. Experimental procedure

The kinetics of phase reversal transformation are examined by performing a series of heat treatments. The experiments were performed on 0.3 mm thick AISI 301 FS sheet of the company ZAPP, with chemical composition (in wt%) of Fe–0.1C(max)–0.9Si(max)–16.7Cr–6.6Ni–0.3Mo. Tensile strength of the material is between 1900 and 2100 MPa containing approximately 65% mechanically induced martensite, the remainder consisting of severely work-hardened *retained* austenite.

The characterization of the reverse transformation is accomplished by subjecting thin sheet metal samples to temperatures ranging from 600 °C to 850 °C for holding times ranging from 0 s till 100 s using a novel laser heat treatment setup. Before *and* after each experiment the martensite-content is measured by a Ferritescope (Fisher MP30, probe FGAB1.3-Fe). The measurements were converted to martensite percentage using the calibration curve provided by Peterson [21], in combination with the thickness compensation as mentioned in the instruction manual of the MP30. The measurement area was sufficiently large to avoid a correction factor for Ferritescope edge effects, see Fig. 1. In all cases a high heating rate was employed and every experiment was performed at least three times.

2.1. Laser heat treatment setup

The heat treatments were performed on a novel laser heat treatment setup. It is capable of reaching the high heating rates of the targeted

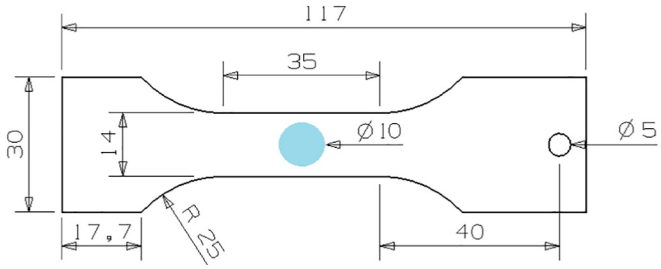

Fig. 1. Geometry of sample and geometry of laser spot (blue) (mm).

industrial processes by direct laser heating of the experimental samples. Heat treatment experiments are generally performed on setups based on resistance heating (see e.g. Somani et al. [22]) or induction heating (see e.g. Löbbe et al. [23]). Yet, the authors chose to develop and construct a laser heating setup because of the availability of the laser-source, expertise and the ease with which the heating rate can be scaled, e.g. by altering the focus of the spot or simply installing a laser with a higher power. Furthermore, it was found that a laser based heating method allows the phase reversal experiments to be conducted on the as-received cold rolled thin sheet metal with relative ease. This has the advantage of being able to test samples with the unique as-received microstructure and texture which can have a large effect on phase reversal behaviour [11]. With such a setup, it becomes straightforward to perform heat treatments on new materials as they are introduced by suppliers (which are not inclined to disclose their cold rolling schemes). In the next paragraphs several aspects of the laser setup are reviewed, including its performance with respect to the temperature homogeneity of the sample during heat treatments.

The laser heat treatments were performed by irradiating the narrow section of a tensile specimen with a spot of 10 mm diameter, see Fig. 1. The intensity-distribution of the spot was homogenized by passing a gaussian collimated spot through a Diffractive Optical Element (DOE) of the company Holo/Or (type RH-217-K-Y-A). The DOE transforms the output of the fiber coupled 2 kW Diode Laser (DF020 HQ - ROFIN) into a flat-top intensity distribution of approximately 10 mm. After holding the temperature of the sample for the desired time, the samples were water quenched. The setup enables typical heating and cooling rates of 1000 K/s and 2000 K/s respectively. Samples cannot be clamped on both sides during heating as this leads to buckling caused by thermal expansion. Therefore, the lower part of the samples was left free, except for a small pretension to keep the sample straight (≈2.5 MPa). A schematic of the test-setup is shown in Fig. 2. Temperature control was realized by spot welding a type-k thermocouple to the back side of the sample, at the center location of the irradiated spot, serving as a feedback for the proportional–integral–derivative control of the heat treatment. Measurement of the in-plane temperature development

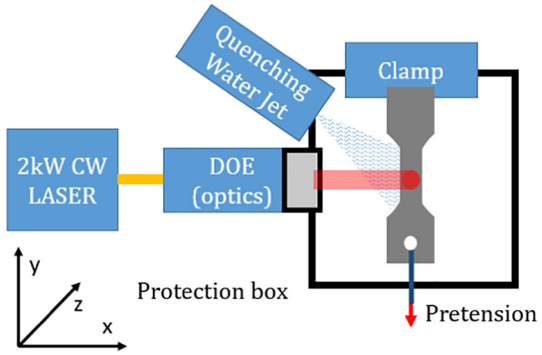

Fig. 2. Schematic of the test setup.

revealed a maximum temperature difference of 35 °C between center and outside of the required spot[1] during heating, which disappears quickly upon holding the temperature constant. The temperature development through thickness cannot be measured reliably therefore it was estimated using FE analysis, this revealed that the temperature delta through thickness is negligible; during heating it is ≈9 °C, during holding it is ≈1 °C.

3. Kinetic model

The kinetic model consists of a combination of a temperature dependent athermal and implicitly time-dependent isothermal transformation. It is presented in rate-form to be able to account for arbitrary thermomechanical loading. The model concept is presented in Fig. 3. In this graph two curves are depicted, the red curve represents athermal transformation, the blue curve isothermal transformation saturation. With infinite heating rate only athermal transformation takes place. In this case there is no time for additional isothermal transformation and therefore the red curve represents the minimum fraction of austenite at a certain temperature. The isothermal saturation line (blue) is reached after prolonged exposure to high temperature. In accordance with Leblond and Devaux [24] the isothermal transformation saturation is the temperature dependent equilibrium fraction of austenite. During an arbitrary heat treatment the transformed fraction will lie between these two curves. The contribution of isothermal versus athermal transformation is governed by the heating rate *and* the rate of isothermal transformation.

3.1. Kinetic modelling

Depending on the heating rate and the temperature of the heat treatment the reverse kinetics may be governed by isothermal transformation, athermal transformation, or a combination of the two. As said, the current model will assume that the transformation is a combination of the two and therefore the interaction between the two transformations must also be accounted for. The overall transformation rate is given by:

$$\frac{df^{\gamma}}{dt} = \frac{df^{\gamma_i}}{dt} + \frac{df^{\gamma_a}}{dT}\frac{dT}{dt} \tag{1}$$

where f^{γ} is the overall austenite volume fraction and f^{γ_a} and f^{γ_i} are the athermally and isothermally formed volume fractions. Note that the initial austenite fraction ($f_0^{\gamma} = 0.35$) represents the *retained* austenite.

3.1.1. Athermal transformation kinetics

An often employed model for athermal transformation processes was presented in 1959 by Koistinen and Marburger [25]. It is a phenomenological model that has only two parameters. In the case of martensite to austenite phase reversal these are the parameters governing the athermal austenite start temperature A_a (threshold temperature for athermal transformation) and a parameter governing the evolution of the athermal transformation with temperature k_a. The formulation is given by:

$$\frac{df^{\gamma_a}}{dT} = \begin{cases} k_a \exp\left(-k_a(T-A_a)\right) & \text{if } f^{\gamma} < f_p^{\gamma_a} \text{ and } T > A_a \\ 0 & \text{otherwise} \end{cases} \tag{2}$$

where, $T > A_a$ enforces the equation to be used in the valid range and $f_p^{\gamma_a}$ represents the minimum austenite fraction (as governed by athermal transformation) that can exist at a certain temperature. It is the red curve in Fig. 3 and is described by:

[1] A spot the size of the probe tip of the Ferritescope i.e. ø6 mm.

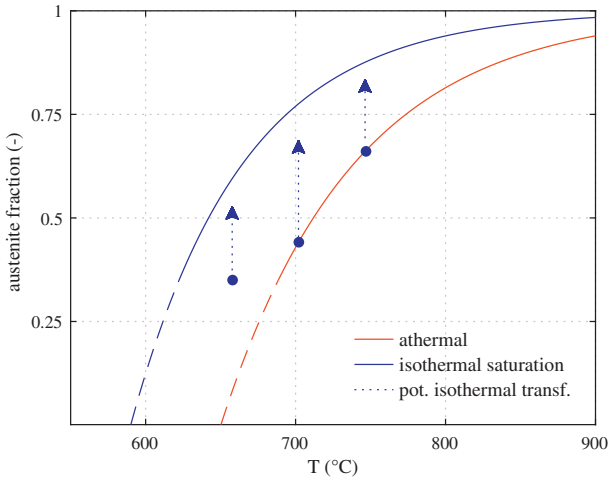

Fig. 3. Explanation of the concept of the kinetic model where the red curve is the potential athermal transformation (Eq. (3)), the blue curve the isothermal transformation saturation (Eq. (6)) and the dotted blue lines represent potential isothermal transformations (Eqs. (4 and (5)). There is no transformation below 0.35 (dashed) since this is the already present retained austenite.

$$f_{\mathrm{p}}^{\gamma_{\mathrm{a}}} = 1 - \exp\left(-k_{\mathrm{a}}(T - A_{\mathrm{a}})\right) \tag{3}$$

Comparing the current volume fraction of austenite with the athermal transformation potential ensures that athermal transformation can take place only when the untransformed volume fraction is below the temperature-dependent athermal transformation potential and that the combined athermal and isothermal transformation does not exceed 100%.

3.1.2. Isothermal transformation kinetics

In principle time dependent transformations can proceed by diffusion and by diffusionless mechanisms, e.g. Machlin and Cohen [26] and Anandaswaroop and Raghavan [27] found isothermal diffusionless martensitic transformation upon quenching of certain quench-hardenable alloys. Lee et al. [28] performed an experimental investigation of isothermal reverse transformation and found evidence that it is not governed by this type of mechanism, but by a thermally activated nucleation and growth mechanism.

Leblond and Devaux [24] described a time-implicit rate equation for modelling isothermal transformation. It considers that the minimum of the free enthalpy of the phase-mixture determines the equilibrium fraction-distribution. If the temperature of the material is increased towards a particular temperature with infinitely slow heating rate the equilibrium fraction is obtained instantaneously. However, as the heating rate towards this temperature is increased, it is observed that there is a retardation with respect to reaching the equilibrium portion. The main features of this model exactly match the observations for isothermal transformation, i.e. time-dependent transformation towards a saturation level. As mentioned, the model is time-implicit and thus suitable for modelling transient laser heat treatments. The description of the isothermal transformation rate is written as:

$$\frac{\mathrm{d}f^{\gamma_{\mathrm{i}}}}{\mathrm{d}t} = \left(f_{\mathrm{s}}^{\gamma_{\mathrm{i}}} - f^{\gamma_{\mathrm{i}}}\right)k \tag{4}$$

where

k represents a reciprocal time and incorporates the temperature dependence of the rate of isothermal transformation. Furthermore, $f^{\gamma_{\mathrm{i}}}$ is the current isothermally formed austenite fraction and $f_{\mathrm{s}}^{\gamma_{\mathrm{i}}}$ is the current temperature-dependent isothermal saturation fraction. The temperature dependence of k is described by an Arrhenius equation:

$$k = \frac{1}{\tau_0}\exp\left(\frac{-Q_\tau}{RT}\right) \tag{5}$$

in which τ_0 is the characteristic time of transformation, Q_τ is the activation energy for isothermal transformation, R is the universal gas constant and T is the temperature in Kelvin.

In accordance with observation, the temperature dependence of the isothermal transformation saturation is described by an exponential relation of the form:

$$f_{\mathrm{s}}^{\gamma_{\mathrm{i}}} = 1 - \exp\left(-k_{\mathrm{s}}(T - A_{\mathrm{s}})\right) \text{ if } T > A_{\mathrm{s}} \tag{6}$$

where k_{s} governs the evolution of the isothermal transformation saturation with temperature and A_{s} governs the start of the saturation curve.

4. Results and discussion

4.1. Model calibration and experimental results

In the previous section, six equations were presented that together comprise the full kinetic model that must be solved numerically. The kinetic model features six parameters of which two describe athermal transformation and four describe isothermal transformation. The calibration of the model parameters is obtained by performing a least squares optimization and by using the *actual* heating curve measurement of each experiment instead of assuming isothermal temperature curves. This has the benefit of being able to predict potential transformation *during* the heating stage of an experiment and it minimizes the effect of experimental temperature variations on the outcome of the model parameters. As mentioned, a non-isothermal experiment was performed; this experiment is excluded from the calibration. The parameters resulting from calibration are shown in Table 1.

The results of the experiments are depicted in Fig. 4. They show that the transformation to austenite is significantly dependent on time and that there is a rapid progression of transformation in the initial stages of the heat treatments. Additionally, it seems that the transformation saturates on a temperature dependent level, at least for the purpose of industrial application of laser heat treatments.

The colored lines in Fig. 4 feature the model prediction. It can be seen that the agreement between experiment and model is very good (goodness–of–fit will be presented and discussed further in Fig. 8 and Table 3). The current experiments include *intermediate temperature–long duration* and *high temperature–short duration*, to explore both potential isothermal and athermal transformation. The fit of the model to experiments of shortest duration is re-illustrated in Fig. 5a and shows good agreement. The time versus temperature graphs of these experiments are shown in Fig. 5b; they emphasize the performance of the setup and the nature of the fastest experiments which subject the samples to extreme heating-rates and quenching-rates. Combined, Figs. 4, 5a and b stress the point that both isothermal and athermal transformation need to be accounted for in the kinetic model. For the heat treatment with target temperature 830 °C (the dark red-topmost curve in Fig. 5b) the kinetic model predicts an almost purely athermal transformation of 49.3%, versus an isothermal transformation of 2.2%, whereas heat treatments performed at 660 °C for long duration are almost purely governed by isothermal transformation. The time during the shortest duration experiments is simply insufficient for a thermally activated transformation to proceed and the transformed fraction can

Table 1
Model parameter values, calibrated by least squares optimization to the Feritscope reverse transformation data.

k_{a}	$1.1\ 10^{-2}$ K^{-1}	τ_0	$1.86 \cdot 10^{-4}$ s	k_{s}	$1.2 \cdot 10^{-2}$ K^{-1}
A_{a}	916 K	Q_τ	85 kJ/mol	A_{s}	853 K

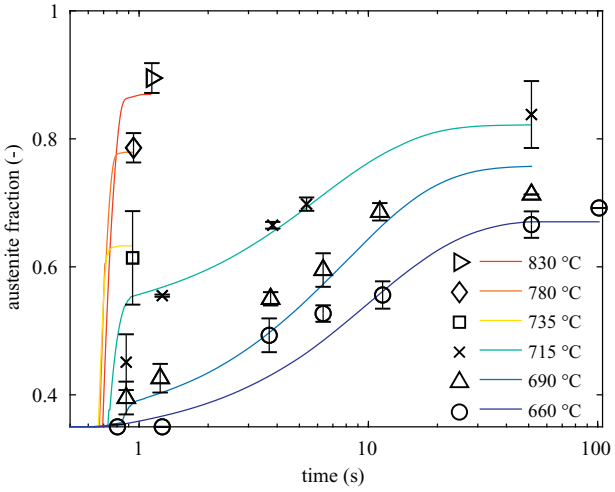

Fig. 4. Reverse transformation experiment (markers) vs model (lines); error bars are ±1 standard deviation.

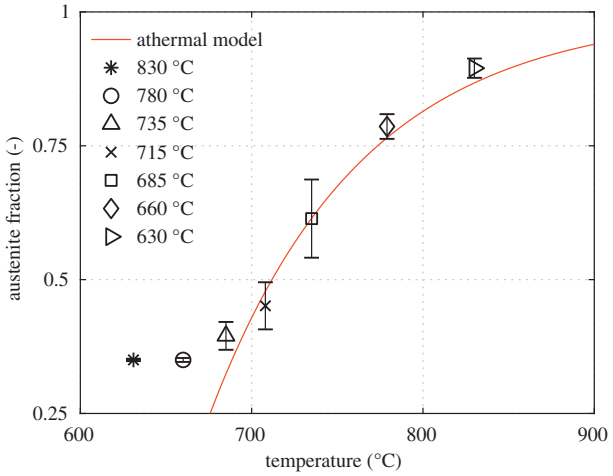

Fig. 6. Athermal model (solid line) compared to the experiments of shortest duration.

be better explained by an athermal transformation mechanism. Note that the apparent time-dependence of the transformation seen in Fig. 5a stems from the time-dependent rise in temperature; the athermal transformation itself is *not* dependent on time.

In Fig. 6, the athermal potential function ($f_p^{\gamma_a}$) is plotted versus all experiments of shortest duration. This shows the good match between the proposed athermal transformation model and the behaviour seen in these experiments. The athermal start temperature (A_a) is the temperature at which this material would initiate transformation when *fully* martensitic. The observed athermal transformation temperature for the current initial state of 35% retained austenite is 670 °C and matches well with experiments reported in the literature [12].

4.2. Added value of a rate-formulation and robustness check of kinetic model

It was shown that there is good agreement between the calibration experiments and the predictions of the proposed model. In Section 4.1 the model has been calibrated using experiments involving fast heating to a single temperature and then holding that temperature for a particular time followed by quenching. These type of experiments are good for calibration and visualization of the transformation kinetics. However real industrial laser heat treatments can have a much more complex thermal loading. As a first step towards validating the proposed model a test is presented to check if the model is capable of predicting the transformation kinetics of such a complex thermal loading history. The experiment in question involves fast heating to 675 °C, holding for 2.5 s, followed by fast heating from 675 °C to 700 °C, then holding for another 7.5 s followed by quenching. The results of the model and the experiment are depicted in Fig. 7a. This comparison shows that there is a good match between predicted austenite fraction and the experimental result for this complex load case. Additionally, Fig. 7a shows a lower and upper bound prediction if the experiment would have been conducted at a single temperature of either 675 °C or 700 °C (see Fig. 7b for the time versus temperature curves involved). It is clear that the predicted lower and upper bound austenite fraction fall outside of the error bars of the experiment. This shows that despite of the small difference in temperature between 675 °C and 700 °C, it is still essential to capture the intermediate transformation rate increase if accurate results are desired; it is therefore a good showcase for the added value of employing a rate-formulated model. It is important to note that this experiment was not used for calibration of the parameters of the model and it is therefore a good first step towards model validation. The dashed vertical line at 3.5 s shown in Fig. 7a and b – corresponding to 2.5 s holding – highlights the *predicted* change in transformation rate and the introduction of the temperature jump. This change of rate can be predicted *because of* the implicitly time-dependent rate formulation of the isothermal transformation, and is an important attribute for the

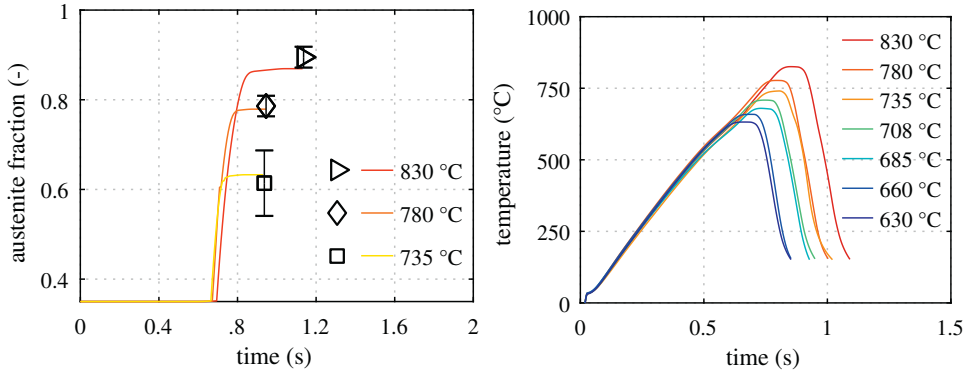

(a) Transformation experiment and modelling. (b) Time vs temperature.

Fig. 5. (a) Close-up of the fit between experiment (markers) and model (solid lines) for the high temperature–short duration experiments. (b) Time versus temperature graphs for the experiments of shortest duration.

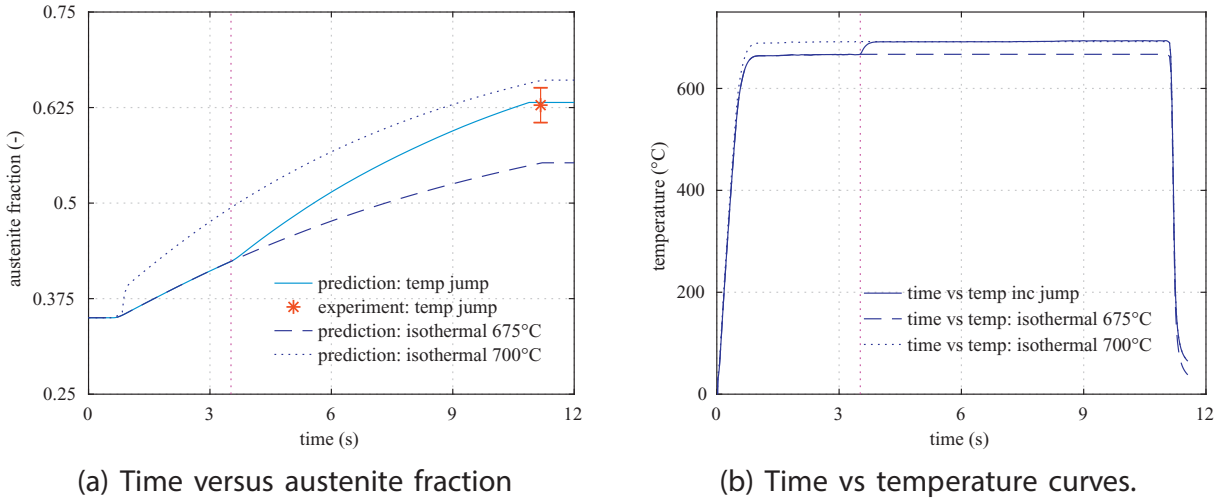

(a) Time versus austenite fraction (b) Time vs temperature curves.

Fig. 7. (a) Comparison between predicted and experimentally obtained austenite fraction after a temperature jump experiment, furthermore upper and lower bound predictions for isothermal experiments at 675 °C and 700 °C. (b) Time versus temperature graphs that were used to generate the model predictions shown in Fig. 7a.

modelling of highly transient laser heat treatments on austenitic stainless steel.

4.3. Added value of modelling both athermal and isothermal transformation

Most of the models that were presented in literature thus far to describe reverse transformation account for isothermal transformation only [12,15,18]. The novelty of the proposed model lies in its ability to account for both athermal and isothermal transformation to better represent the underlying mechanisms and – ultimately – achieve better agreement between data and model.

In this section it is shown that the proposed addition of the athermal mechanism – adding two more fit parameters to the equation – really aids agreement between model and data. This is achieved by excluding the athermal part of the model (Eqs. (2) and (3)) and recalibrating the model parameters to the isothermal part only (Eqs. (4)–(6)). Subsequently the model fit is compared to the data and R^2 and R^2_{adj} are determined. It might be expected that an athermal-only model would be part of the comparison in Fig. 8, yet the goal of this research is to develop a model that is capable of describing reverse transformation that occurs in (fast) transient heat treatment. The transformations occurring in these processes are dependent on time. Although athermal transformation can be significant in such processes, an athermal-only transformation model is not explored since it cannot describe the current experimental observations nor the foreseen processes.

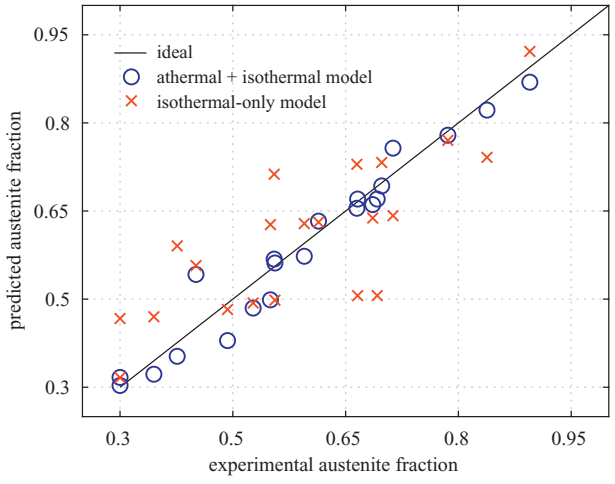

Fig. 8. Residuals of the proposed model (athermal and isothermal model) versus residuals of an isothermal-only model. Datapoints in this plot represent the difference between the mean of three experiments and the corresponding model prediction.

Table 2
Parameter values belonging to the calibration of the isothermal-only model (Eqs. (4)–(6)).

τ_0	$5.6 \cdot 10^{-5}$ s	k_s	$1.33 \cdot 10^{-2}$ K^{-1}
Q_τ	65 kJ/mol	A_s	890 K

Table 3
Comparison of goodness-of-fit statistics for the combined athermal–isothermal model and the isothermal-only model, p is the number of parameters.

Model	p	R^2	R^2_{adj}
Athermal and Isothermal transformation	6	0.95	0.86
Isothermal transformation only	4	0.62	0.23

Fig. 8 displays the residuals of the model predictions for both the complete model – containing both athermal and isothermal transformation – and the isothermal-only model; associated model parameters for the isothermal-only model are shown in Table 2. Clearly the prediction of the complete model that includes the athermal mechanism (blue circle) is much better compared to the prediction of an isothermal only model (red x). In general the isothermal-only model has difficulty in simultaneously predicting the behaviour seen during the two diverse type of tests, i.e. high-temperature short-duration *and* intermediate-temperature long-duration. Table 3 confirms that the model containing both athermal and isothermal transformation performs much better than the isothermal-only model.

5. Conclusion

In this research a novel experimental setup is used with which it is possible to conduct high heating rate laser-based heat treatments. The setup is used to characterize the reverse transformation of AISI 301 at heating rates that are relevant for industrial laser heat treatments. Furthermore, a novel extended rate-dependent time-implicit kinetic model is presented and an initial robustness check is performed by comparing

the model prediction to an independent non-isothermal experiment. It was shown that:

- The extended kinetic model is capable of reproducing the observed kinetics with high accuracy and the combination of athermal and isothermal transformation mechanisms is essential for obtaining the level of agreement that is achieved.
- Saturation of isothermal transformation is apparent even when holding times of reverse heat treatments are limited to 100 s and should therefore be accounted for when modelling isothermal reverse transformation.

Data availability

The raw/processed data required to reproduce these findings cannot be shared at this time due to technical or time limitations. Relevant data can be made available on request via the corresponding author's email.

CRediT authorship contribution statement

H. Kooiker: Conceptualization, Investigation, Methodology, Validation, Visualization, Writing - original draft, Writing - review & editing. **E.S. Perdahcıoğlu:** Conceptualization, Methodology, Writing - review & editing. **A.H. van den Boogaard:** Conceptualization, Methodology, Writing - review & editing.

Declaration of Competing Interest

None.

Acknowledgements

The authors want to thank Philips HealthTech for the financial support that enabled this research. Furthermore, the authors want to express their sincerest gratitude to Ronald van der Linden for his help in building the novel laser heat treatment setup.

References

[1] R.D.K. Misra, R.D.K. Nayak, S.A. Mali, J.S. Shah, M.C. Somani, L.P. Karjalainen, Microstructure and deformation behaviour of phase-reversion-induced nanograined/ultrafine-grained austenitic stainless steel, Metall. Mater. Trans. A 40A (2009) 2498.
[2] A. Mateo, A. Zapata, G. Fargas, Improvement of mechanical properties on metastable stainless steels by reversion heat treatments, IOP Conference Series: Materials Science and Engineering, vol. 48, IOP Publishing 2013, p. 012001.
[3] M. Moallemi, A. Zarei-Hanzaki, S.-J. Kim, H. Alimadadi, On the microstructural-textural characterization and deformation analysis of a nano/ultrafine grained Fe-20Cr-8Mn-0.3N duplex alloy with superior mechanical properties, Mater. Charact. 156 (2019) 109878.
[4] G. Kubla, E. Hornbogen, Causes of partial or complete reversibility of martensitic transformation in alloys of iron, Le J. de Physique IV 5 (C2) (1995) 305–310.
[5] K. Tomimura, S. Takaki, S. Tanimoto, Y. Tokunaga, Optimal chemical composition in Fe-Cr-Ni alloys for ultra grain refining by reversion from deformation induced martensite, ISIJ Int. 31 (1991) 721–727.
[6] H. Kessler, W. Pitsch, On the nature of the martensite to austenite reverse transformation, Acta Metall. 15 (1967) 401–405.
[7] Y.-K. Lee, H.-C. Shin, D.-S. Leem, J.-Y. Choi, W. Jin, C.-S. Choi, Reverse transformation mechanism of martensite to austenite and amount of retained austenite after reverse transformation in Fe-3Si-13Cr-7Ni (wt-%) martensitic stainless steel, Mater. Sci. Technol. 19 (2003) 393–398.
[8] D.P. Yang, D. Wu, H.L. Yi, Reverse transformation from martensite into austenite in a medium-mn steel, Scr. Mater. 161 (2019) 1–5.
[9] P. Dastur, A. Zarei-Hanzaki, R. Rahimi, M. Moallemi, V. Klemm, B.C. de Cooman, J. Mola, Martensite reversion duality behaviour in a cold-rolled high mn transformation-induced plasticity steel, Metall. Mater. Trans. A 50 (2019) 4550–4560.
[10] I.R. Souza Filho, A. Kwiatkowski da Silva, M.J.R. Sandim, D. Ponge, B. Gault, H.R.Z. Sandim, D. Raabe, Martensite to austenite reversion in a high-mn steel: partitioning-dependent two-stage kinetics revealed by atom probe tomography, in-situ magnetic measurements and simulation, Acta Materialia 166 (2019) 178–191.
[11] K. Tomimura, S. Takaki, Y. Tokunaga, Reversion mechanism from deformation induced martensite to austenite in metastable austenitic stainless steels, ISIJ Int. 31 (1991) 1431–1437.
[12] M.C. Somani, P. Juntunen, L.P. Karjalainen, R.D.K. Misra, A. Kyröläinen, Enhanced mechanical properties through reversion in metastable austenitic stainless steels, Metall. Mater. Trans. A 40 (2009) 729–744.
[13] D. Johannsen, A. Kyrolainen, P. Ferreira, Influence of annealing treatment on the formation of nano/submicron grain size AISI 301 austenitic stainless steels, Metall. Mater. Trans. A 37 (2006) 2325–2338.
[14] A. di Schino, M. Barteri, J.M. Kenny, Development of ultra fine grain structure by martensitic reversion in stainless steel, J. Mater. Sci. Lett. 21 (2002) 751–753.
[15] S. Rajasekhara, P.J. Ferreira, Martensite → austenite phase transformation kinetics in an ultrafine-grained metastable austenitic stainless steel, Acta Mater. 59 (2011) 738–748.
[16] V. Erukhimovitch, J. Baram, Nucleation and growth transformation kinetics, Phys. Rev. B 51 (1995) 6221.
[17] M. Stalder, S. Vogel, M.A.M. Bourke, J.G. Maldonado, D.J. Thoma, V.W. Yuan, Retransformation ($\alpha \rightarrow \gamma$) kinetics of strain induced martensite in 304 stainless steel, Mater. Sci. Eng. A 280 (2000) 270–281.
[18] E.I. Galindo-Nava, W.M. Rainforth, P.E.J. Rivera-Díaz-del Castillo, Predicting microstructure and strength of maraging steels: elemental optimization, Acta Mater. 117 (2016) 270–285.
[19] H.K. Yeddu, T. Lookman, A.B. Saxena, Reverse phase transformation of martensite to austenite in stainless steels: a 3d phase-field study, J. Mater. Sci. 49 (2014) 36423651.
[20] X. Zhang, G. Shen, C. Li, J. Gu, Phase-field simulation of austenite reversion in a Fe-9.6Ni-7.1Mn (at.%) martensitic steel governed by a coupled diffusional/displacive mechanism, Mater. Des. 188 (2020) 108426.
[21] J. Talonen, P. Aspegren, H. Hänninen, Comparison of different methods for measuring strain induced α-martensite content in austenitic steels, Mater. Sci. Technol. 20 (2004) 1506–1512.
[22] M.C. Somani, M. Jaskari, S. Sadeghpour, C. Hu, R.D.K. Misra, T.T. Nyo, L.P. Karjalainen, Improving the yield strength of an antibacterial 304cu austenitic stainless steel by the reversion treatment, Mater. Sci. Eng. A 793 (2020) 139885.
[23] C. Löbbe, O. Hering, L. Hiegemann, A.E. Tekkaya, Setting mechanical properties of high strength steels for rapid hot forming processes, Materials 9 (2016) 229.
[24] J.B. Leblond, J. Devaux, A new kinetic model for anisothermal metallurgical transformations in steels including effect of austenite grain size, Acta Metall. 32 (1984) 137–146.
[25] D.P. Koistinen, R.E. Marburger, A general equation prescribing the extent of the austenite-martensite transformation in pure iron-carbon alloys and plain carbon steels, Acta Metall. 7 (1959) 59–60.
[26] E.S. Machlin, M. Cohen, Isothermal mode of the martensitic transformation, J. Met. 4 (5) (1952) 489–500.
[27] A.V. Anandaswaroop, V. Raghavan, Isothermal martensite formation in an Fe-Ni alloy, Scr. Metall. 3 (1969) 221–224.
[28] S. Lee, Y. Park, Y. Lee, Reverse transformation mechanism of martensite to austenite in a metastable austenitic alloy, Mater. Sci. Eng. A 515 (2009) 32–37.